Prediction of Tribological Behaviour of AA5083/CSA-ZnO Hybrid Composites Using Machine Learning and Artificial Intelligence Techniques

A. Nagaraj, S. Gopalakrishnan, M. Sakthivel, and D. Shivalingappa

Abstract Aluminium Alloys AA5083 dispersed with varying fractions of reinforcement was fabricated through the stir casting method. In varying weight percentage combinations, zinc oxide (ZnO) and coconut shell ash (CSA) particles were combined to create hybrid reinforcement particles. Using a pin-on-disc tribometer, the wear characteristics of the developed AA5083 hybrid composites were estimated. The volumetric proportion of hybrid reinforcement particles CSA (3, 6, 9 and 3 ZnO wt%), load (20, 30, 40 N), sliding velocity (2, 3, and 4 m/s), Cumulative Time (4.16, 5.55, and 8.33 min), and sliding distance are some of the experimental parameters (1000 m). Wear analysis revealed effective bonding and homogeneous dispersion of hybrid reinforcement particles onto the AA5083. Analysis of Specific Wear Rate (SWR) results showed that Specific Wear Rate rose with load, sliding velocity, and sliding duration while decreasing with hybrid particle dispersion. This research proposes the use of several intelligent classification techniques using Machine Learning (ML) and Artificial Neural Network (ANN) to predict the wear rate of an AA 5083 hybrid composite. For estimating wear quantities, the algorithms Random Forest (RF), Neural Network (NN), and k-nearest neighbours (kNN) are utilized. Six inputs are utilized to train and evaluate the Machine Learning (ML) algorithms: the Applied Load (N), Sliding Velocity, Sliding Speed, Cumulative Time, Percentage of Reinforcements, and Sliding Distance. The output is the Specific Wear Rate (SWR). The

A. Nagaraj (✉)
Associate Professor, Department of Mechanical Engineering, Star Lion College of Engineering and Technology, Thanjavur 614206, India
e-mail: naga.nagaraj.raja@gmail.com

S. Gopalakrishnan
Department of Mechanical Engineering, K. S. Rangasamy College of Technology, Thiruchengode 637215, India

M. Sakthivel
Department of Mechanical Engineering, Adhiyamaan College of Engineering, Hosur 635109, India

D. Shivalingappa
Department of Mechanical Engineering, B. N. M. Institute of Technology, Bengaluru 560070, India

S. B. Boppana et al. (eds.), *Structural Composite Materials*, Composites Science and Technology, https://doi.org/10.1007/978-981-99-5982-2_12

RF, NN, and KNN algorithms all produced success rates of correlation between experimental to anticipated of 0.90, 0.84, and 0.90, respectively. The same model data was utilised to train and evaluate Artificial Neural Networks (ANN), with the Multilayer Perceptron (MLP) network having the lowest Mean Square Error (MSE) to improve machine learning prediction accuracy. Maximum estimate error range of 0.1%, training and cross-validation of 0.00000496 and 0.0261, respectively, with linear correlation coefficient in testing of 0.9999 or 99.9% better prediction accuracy rate. The AA 5083 composites were designed and implemented using this machine learning and artificial neural network model for forecasting specific wear rate.

Keywords AA 5083 · Stir casting · Hybrid composites · Wear · Machine learning (ML) · Artificial Neural Network (ANN)

1 Introduction

Aluminium Metal Matrix and Hybrid Composites (AMMHCs) are used in aerospace, automotive, ballistic, electrical, aviation, tribological, space and air vehicle, thermal, structure, defence industries, military, transportation, engineering, and mineral processing applications due to their high strength-to-weight ratio, good corrosion, oxidation, and wear resistance, and high thermal conductivity [1].

Due to extensive passivation, aluminium (Al) is one of the most frequently utilised metals in industries. It is a very strong, wear- and corrosion-resistant alloy that is lightweight. By changing their elemental compositions, aluminium alloys may have improved chemico-physical properties. To create varied concentrations of defect-free and evenly dispersed aluminium composites, stir casting technology is often used. AA5083 Due to its light weight, fabricability, physical characteristics, corrosion resistance, and affordability, aluminium–magnesium alloys are often utilised in the aerospace, automotive, shipbuilding, and construction sectors. The majority of aluminium–magnesium alloys, nevertheless, seem to have minimal wear resistance. There have been some recent findings on the tribological behaviour of different aluminium alloys [2].

Zhang and Li investigated the impact of yttria addition on aluminum's wear resistance in dry and corrosive environments. They discovered that the scattered yttria particles significantly improved the aluminium matrix composites resistance of aluminum to corrosion, corrosive and dry wear [3].

The use of agricultural waste (rice husk ash, coconut shell ash, bagasse ash, and corn cob ash), industrial waste (fly ash), or recycled materials has been a new breakthrough in composite materials. Agro-waste products that have been reinforced have appealing qualities including cheap cost, low density, and less environmental contamination. Coconut shell ash (CSA) particles are used extremely seldom, despite the fact that many studies have researched the improvement of mechanical characteristics of AMCs by the inclusion of agro-wastes. The authors' decision to concentrate on

creating high-performance aluminium matrix composites with reinforcements made from coconut shell ash was driven by the paucity of existing research [4].

Zinc oxide (ZnO), an n-type semiconductor, is a very interesting material because it can be used to make solar cells, sensors, displays, gas sensors, varistors, piezoelectric devices, electro-acoustic transducers, photodiodes, UV light emitting devices, and antibacterial materials [5]. Due to its distinctive mechanical, electrical, and optical characteristics as well as its many uses, zinc oxide (ZnO) is a significant substance in the metal oxide family [6]. The mechanical characteristics of the extruded Mg materials are improved by the addition of modest volume fractions of nano-particulate reinforcements such as nano-Al_2O_3, nano-ZnO, to pure Mg/alloys [7].

This study looked at how ZnO particles affected the stir-cast aluminium metallic matrix composite's compressive strength, hardness, and wear properties. The reinforcement included various weight percentages of ZnO (0, 2, 4, 6, 8 and 10) with wear characteristics that improve as the weight percentage of ZnO rises. For specimens of aluminium reinforced with 2, 4, 6, 8, or 10 weight percent ZnO particles, the increases in Brinell hardness are (15%), (25%), (35%), (40%), and (50%) accordingly. It was discovered that by increasing the zinc oxide content and going above the composite minimum quantity, which reflects the overall percentage of zinc oxide, the volume loss was significantly decreased (10 percent) [8].

Aluminium matrix composite with graphite and Coconut Shell Ash (CSA). Modified stir-casting creates Al-1100 composites. Three more Aluminium with Aluminium oxide, Aluminium–Aluminium oxide–Graphite, and Aluminium-Coconut Shell Ash composites were developed. The Al-CSA composite outperforms the other three composites in terms of mechanical and tribological characteristics including tensile strength and hardness. Gr incorporation aids in the hybrid Al-CSA-Gr composite's improved tribological characteristics while allowing for a somewhat lower specific strength [9].

Composites A and B with Al-5083 matrices reinforced with 5 and 10% wt% B4C particles were manufactured by cryomilling and consolidating. Composite pins were tested for dry sliding wear using a pinon-disc tribometer. Composite B (10 wt% B4C) wore 40% less than composite A (5 wt% B4C) under the identical circumstances. This experiment suggests that B4C particles improve composites wear resistance [10].

After ECAE, the alloy's wear resistance rose with the least amount of mass loss and friction coefficient. As a result of ECAE processing, the alloy is now resistant to scratch deformation. The mechanical and wear characteristics of aluminium 5083 alloy were improved via ECAE processing. The alloy may now be used in a variety of technical applications that call for high strength because to improvements in its mechanical and wear qualities [11].

According to wear experiments, the Al 5083/SiCp nanocomposite has a much lower specific wear rate than the nanostructured Al 5083 alloy. In contrast to Al5083/SiCp, which showed a wear mechanism of adhesive wear to abrasive wear, nanostructured Al5083 alloys had a mix of abrasive and delamination wear processes [12].

There have not been many research specifically looking at coconut shells in metal matrix composite. A low-weight metal matrix composite with high thermal and wear resistance has been produced using CSAp in certain studies [13].

The Al 6063 alloy/coconut shell composites mechanical and corrosion characteristics. They observed an improvement in hardness and tensile strength as coconut shell % weight increased and corrosion resistance decreased [14]. Similar results were obtained when coconut shell was used to enhance recycled scrap aluminium's mechanical and wear qualities [15].

Machine-Learning (ML) techniques have recently been used to anticipate the characteristics of metallic materials. ML models, for instance, may be used to look for shape memory alloys with certain transition temperatures [16]. A method for designing materials that combine tests with ML models to create high-entropy alloys with high toughness. A deep neural network was used by Feng et al. to forecast the flaws in stainless steel. ML models to forecast the capacity of binary metallic alloys to make glass. The design of tailored metallic glasses was confirmed using commercially feasible manufacturing techniques using a machine learning framework for speeding design. High-throughput experimentation and machine learning-based iteration to quickly find novel glass-forming systems ML techniques have been used in many research to determine the relationships between an alloy's capacity to produce glass and its empirically observed characteristics [17]. Thus, these experiments provided conclusive evidence that ML techniques were effective and dependable for identifying novel metal matrix composites and predicting their properties.

Random Forests are trained using bootstrapped datasets of the same size as the training set (RF). Randomly resampling the training set produces these datasets. Once a tree is generated, out-of-bag (OOB) samples are used as the test set. OOB generalization error estimate is all test sets' categorization error rate. Bagged classifiers have the same OOB error as using a training-set-sized test set. OOB estimation no longer requires a separate test set. Each CART tree votes for one class, and the forest predicts the class with the most votes to categorize input data [18].

A mathematical or computer model called a neural network replicates the structure and functionality of a biological neural network. It uses artificial neurons to process information in a connectionist manner. Modern neural networks are non-linear statistical modelling tools that are often used for simulating intricate relationships between input and output while looking for patterns in data. The neural network approach is based on the same assumptions as how the human brain functions. The human brain has a vast network of neurons that link sensory and motor nerves. The majority of scientists thought that neurons in the brain communicate with one another by firing electrical impulses across synapses [19].

A broad family of algorithms used in classification, regression, and density estimation is called artificial neural networks (ANN-s). A function known as a Multilayer Perceptron (MLP) may be imagined as a network made up of multiple layers of neurons coupled in a feedforward fashion. Input neurons are the neurons that represent input variables in the first layer. The output neurons in the top layer are those that deliver the function result value. Hidden layers are those layers that exist between the first and final levels. Every neuron in the network acts as a perceptron, accepting

input values x1, x2, … xk and using the formula to calculate output value o;

$$O = \emptyset \sum_{i=1}^{k} (\text{wixi} + \text{b}) \tag{1}$$

where wi, b are the neuron's weights and bias, and is a nonlinear function. (x) is 1 / 1 + e ax or tanh (x). The multilayer perceptron is trained by finding the weights and biases of all the neurons that will result in the network having the least amount of error on the training set. A nonlinear decision border between classes is modelled by the multilayer perceptron, a nonlinear classifier. Since the training data we employed was linearly separable, as was discussed in the preceding section, using a nonlinear decision boundary had little chance of enhancing generalization performance. As a consequence, the basic perceptron's output is the best one we could hope for. Another issue in our situation is that a network with 20,000 input neurons makes it difficult to perform effective backpropagation learning. Therefore, reducing the number of features to a manageable number would be the only practical approach to deploying multilayer perceptron [20].

The k-NN method is the most fundamental ML technique, and it may be used for both classification and regression. To put it simply, k-NN uses the average of the object's k-NNs as the property value for regression purposes. It is common practise to utilise K-NN to predict forest attributes from data collected across disciplines. The distance measure and closest neighbour weighting used in k-NN implementations are also factors. The accuracy and efficiency of computations depend on accurately determining k. To determine the best value for k, we employed a combination of the leave-one-out (LOO) cross-validation technique and the v-fold (dividing training samples into two v-fold halves, v − 1 for prototype and one fold for validation) (1–20). For the k-NN estimator, the LOO is a recognized technique for producing unbiased estimates of predicted classification or estimation error. In this method, the algorithm selects k with the lowest RMSE after computing RMSE in validation sample sets for each value of k [21].

To assess the wear resistance of abrasion-resistant tribological materials to be employed under various operating circumstances, several research are needed. These tests may take a long period. Thus, there has been a growing need to create machine learning algorithms, such as the ANN-MLP algorithm, which have recently been able to utilize experimental data to anticipate wear behaviours of materials in order to decrease the number of tests and lower the cost of experimental investigations.

2 Materials and Methods

2.1 Preparation of Coconut Shell Ash

The surface skins of the coconut shells were cleaned and smoothed after they were purchased from a nearby market. The material was then crushed and ground in a ball mill and a jaw crusher, respectively. The ground material was separated using 100 mesh-size screens. The powder was burned for three hours at 1200 °C (1473 K). Once again, a ball mill was used to grind the resulting ash. The material was screened to a 240 mesh size (50 μm).

2.2 Preparation of AA5083-Based Hybrid Composites

The matrix alloy chosen for the development of composite material is Al–Mg–Mn alloy and designated by the aluminium association as AA 5083. The chemical compositions of the matrix material are given in Table 1.

Percentage of Zinc oxide and the chemical composition of coconut shell ash burned at 700 degrees Celsius were also identified by XRF, and the results are shown in Table 2.

Aluminium Alloy (grade AA5083) was cut from an ingot and preheated at 300 °C for 1 h. The material is in a 1073 K bottom-pouring furnace (800 °C). Inert Ar prevented oxidation during melting. The furnace's stirrer was controlled by a PID rheostat. Slowly lowering the rotating spindle formed a vortex in the pool. Reinforcement particles were put into the liquid melt vortex at 1223 K (950 °C). The spindle was moved from top to bottom with such a 2-mm clearance. This ensured a smooth melt. Slowly decreasing the melt's temperature between 1123 K (850 °C) and 1023 K (750 °C) increases its viscosity. This retained fine particles in the liquid melt. The liquid that contained the particles was put into a steel mould that had been warmed to 673 K (400 °C). The melting furnace is shown in Fig. 1. Four Aluminium alloy composites, namely AA5083, AA5083-3%CSA-3%ZnO, AA5083-6%CSA-3%ZnO and AA5083-9%CSA-3%ZnO reinforcement were cast under different conditions were added separately with different casting in the form of Table 3.

Table 1 Chemical composition of aluminium (5083) alloy in weight percentage

Constituent	Al	Mg	Cr	Cu	Mn	Fe	Si	Ti	Zn	Others
Percentage	92.6	4.9	0.25	0.1	0.8	0.4	0.4	0.15	0.25	Max 0.20

Table 2 The wt% of CSA and ZnO in the chemical composition

Elements	CSA	ZnO
SiO_2	45.05	–
Cuo	–	7.44
TiO_2	–	0.26
Al_2O_3	15.6	–
Fe_2O_3	12.4	5.68
CaO	0.57	–
MgO	16.2	0.50
SO_3	–	–
K_2O	0.52	0.07
Na_2O	0.45	0.22
ZnO	0.3	84.6
MnO	0.22	0.33
Others	Balance	Balance
LOI	8.69	0.94

3 Experimental Work

From the castings, ASTM test specimens were machined. Three of each test type were performed. Figure 2 demonstrates dry slide wear testing using DUCOM's pin-on-disc apparatus [22].

The pin (workpiece) was against the disc's 105 mm wear track. The disc's pin was deadweight-loaded. Many samples were examined with 20, 30, and 40 N loads at 2, 3, and 4 m/s. Similar wear testing reveals a 1000-m sliding distance. 6 mm pins were 35 mm. Before the test, the pin worm surfaces were slid with an emery sheet to touch the steel disc. The sample and worn track were cleaned with acetone and weighed to 0.0001 g before and after each test [22].

3.1 Microstructure Analysis

The microstructure of cast samples and wear debris surface morphology were examined using a LEICA S440i SEM equipped with an Oxford INCATM EDS system. Before placing the samples in the sample chamber, they were taped on using double-sided carbon tape. The SEM accelerated at 5 to 20 kV.

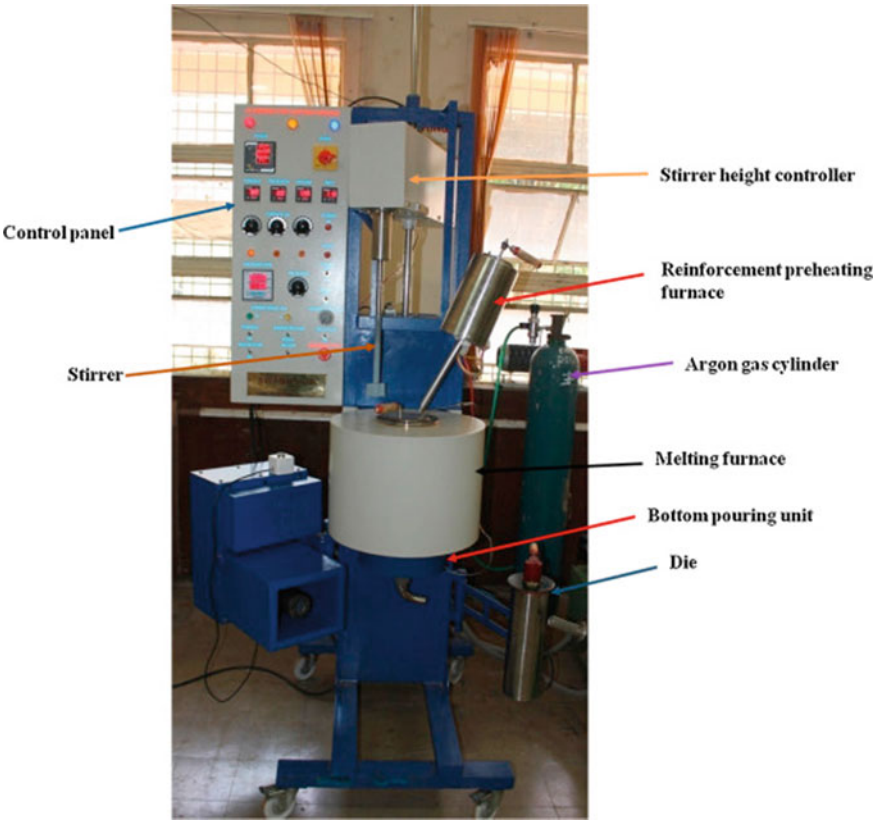

Fig. 1 Melting furnace-stir casting

Table 3 Percentage of AA 5083 hybrid composites

Samples	Aluminium 5083%	CSA %	ZnO %
1	100	0	3
2	94	3	3
3	91	6	3
4	88	9	3

3.2 Architecture of Artificial Neural Networks

An effective data modelling technique that can capture and depict complex input and output interactions is an artificial neural network. Identification of the network architecture, including the number of input and output neurons, hidden layers, and neurons in each hidden layer, as well as the network parameters, is necessary for the construction of ANN models (Activation Function and Learning Rate). Using both

Fig. 2 Pin-on disc wear testing machine

supervised and unsupervised learning techniques, artificial neural networks include at least three layers, an input layer, several hidden layers, and an output layer.

3.3 Inputs and Outputs for ML and MLP-ANN

Six input neurons (Ni = 6) represent the variables of loads (L; N), sliding velocities (v; m/s), sliding speeds (N; RPM), reinforcement percentages (Reinforcement;%), cumulative time (t; mints), co-efficient of friction (μ) for AA 5083 CSA and ZnO hybrid composites. One neuron represents the value of the corresponding Specific Wear Rate (mm^3/N.M) in the output layer. For predicting the Specific Wear Rate of AA 5083 composites, ANN (MLP) was tested. The experimental data sets for Specific Wear Rate are 36 samples.

4 Result and Discussion

4.1 Tribological Behaviour

The tribological behaviour of the hybrid composite with the AA 5083 matrix was followed through several phases. The tests were performed in conditions without lubrication on samples with the best structural, mechanical, and anti-corrosion characteristics. The wear loss was measured during the testing. The wear loss, one of the major parameters for wear monitoring, was estimated based on the volume of worn material, sliding velocity, sliding time, and a constant1000 m sliding distance.

Tribological Sample, Table 4 provides the specific wear rate values for the tested materials based on the loads, sliding velocity, and sliding speed. Due to the extensiveness of the obtained results, a partial number of experimental values of wear loss is shown in Table 4. First, the testing of the base material aluminium alloy AA 5083, was performed, and then 3 wt% CSA, 6 wt% CSA 9 wt% CSA with 3 wt% ZnO was added in the base. The Specific Wear Rate decreased by increasing CSA with 3% percentage reinforcements and increasing load and sliding velocity to the base material of the hybrid composites. The coefficient of friction of the AA 5083 hybrid composites was significantly reduced by adding only 6 wt% CSA and 3% ZnO. With the addition of 3 and 9% CSA, the co-efficient of friction increased while increasing loads and Sliding velocity at certain intervals, while in others it decreased.

4.2 Effect of Applied Loads and Sliding Velocities on Specific Wear Rate and Co-efficient of Friction

The applied load is one of the most important determinants of the specific wear rate of the composites. The unreinforced aluminium 5083 alloy is shown to have a higher specific wear rate than hybrid composites. This is mainly because the hard dispersoids on the surface of the composites function as protrusions and protect the matrix from hard interaction with the counter surfaces, causing hybrid composites to wear less gradually than alloys under all loads. Figure 3 shows that the specific wear rate of the composites decreases with increasing load at a constant sliding distance (1000 m).

At 20 and 40 N loads, the composites containing 6% CSA and 3% ZnO had the lowest specific wear rate. At 30 and 40 N, composites containing 6% CSA and 3% ZnO hybrids exhibited an essentially same specific wear rate. When the load is increased from 20 to 40 N, composites with percentage increases reveal a lower specific wear rate than all the hybrid composites.

From Fig. 4, composites with more reinforcements have stronger wear resistance at 3 m/s sliding velocity, constant sliding distance, and constant load 20 N. This might be because CSA and ZnO particles are easily ploughed away from the matrix's surface, increasing wear at 4 m/s sliding velocity. In hybrid composites containing zinc oxide particles, the particles fragment into small pieces and continue to inhibit particle removal, decreasing wear.

Figures 5 and 6 By incorporating weight percentages of CSA and ZnO, the composites coefficient of friction was significantly lowered. The co-efficient of friction increased in certain periods and decreased in others with the addition of weight percent of reinforcements, increasing load, and sliding velocity.

Table 4 Experimental wear analysis of AA 5083 hybrid composites

Sl. No.	Composition of AA 5083	Load (N)	Sliding velocity (m/s)	Sliding speed (rpm)	Cumulative Time (sec)	Initial mass (m1)	Final mass (m2)	Wear Loss (Δm)	Coefficient of friction (Ff/N) (μ)	Wear rate Δm/L × 10^{-8} (m/L) (N/m)	Volumetric wear rate (wv × 10) [Δm/ρt] (mm^3/s)	Specific wear rate (ws × 10^{-1}) [wv/vs FN] (mm^3/N-m)
1	Pure 5083	20	2	364	8.33	3.4649	3.4566	0.0083	0.6738	8.3	6.2	1.56
2	Pure 5083	30	2	364	8.33	3.4579	3.4487	0.0098	0.6375	9.8	7.4	1.23
3	Pure 5083	40	2	364	8.33	3.4487	3.4389	0.011	0.6388	11	8.3	1.03
4	Pure 5083	20	3	546	5.55	3.4699	3.4649	0.005	0.5825	5	5.6	0.94
5	Pure 5083	30	3	546	5.55	3.4389	3.4317	0.0072	0.645	7.2	8.1	0.9
6	Pure 5083	40	3	546	5.55	3.4317	3.4239	0.0078	0.6625	7.8	8.8	0.73
7	Pure 5083	20	4	728	4.16	3.4848	3.4744	0.0104	0.6075	10.4	15.6	1.95
8	Pure 5083	30	4	728	4.16	3.4744	3.463	0.0114	0.82	11.4	17.1	1.43
9	Pure 5083	40	4	728	4.16	3.4712	3.4588	0.0124	0.6931	12.4	18.6	1.55
10	3% CSA 3% ZnO	20	2	364	8.33	3.1619	3.1546	0.0073	0.7588	7.3	6	1.5
11	3% CSA 3% ZnO	30	2	364	8.33	3.1546	3.1457	0.0089	0.6083	8.9	7.3	1.22
12	3% CSA 3% ZnO	40	2	364	8.33	3.1457	3.1364	0.0098	0.6338	9.8	8.1	1.01
13	3% CSA 3% ZnO	20	3	546	5.55	3.1663	3.1619	0.0044	0.675	4.4	5.4	0.91
14	3% CSA 3% ZnO	30	3	546	5.55	3.1364	3.1311	0.0053	0.6058	5.3	6.5	0.73
15	3% CSA 3% ZnO	40	3	546	5.55	3.1311	3.1249	0.0062	0.6106	6.2	7.7	0.64

(continued)

Table 4 (continued)

Sl. No.	Composition of AA 5083	Load (N)	Sliding velocity (m/s)	Sliding speed (rpm)	Cumulative Time (sec)	Initial mass (m1)	Final mass (m2)	Wear Loss (Δm)	Coefficient of friction (Ff/N) (μ)	Wear rate Δm/L × 10^{-8} (m/L) (N/m)	Volumetric wear rate (wv × 10) [Δm/ρt] (mm^3/s)	Specific wear rate (ws × 10^{-1}) [wv/vs FN] (mm^3/N-m)
16	3% CSA 3% ZnO	20	4	728	4.16	3.1789	3.1707	0.0082	0.6413	8.2	13.5	1.69
17	3% CSA 3% ZnO	30	4	728	4.16	3.1707	3.1667	0.004	0.7175	4	6.6	0.55
18	3% CSA 3% ZnO	40	4	728	4.16	3.1667	3.1652	0.0015	0.8213	1.5	2.5	0.15
19	6% CSA 3% ZnO	20	2	364	8.33	3.2208	3.2134	0.0074	0.8	7.4	5.7	1.43
20	6% CSA 3% ZnO	30	2	364	8.33	3.2124	3.2035	0.0089	0.5767	8.9	6.9	1.15
21	6% CSA 3% ZnO	40	2	364	8.33	3.2026	3.1916	0.0093	0.5113	9.3	7.2	0.9
22	6% CSA 3% ZnO	20	3	546	5.55	3.225	3.2208	0.0042	0.6363	4.2	4.9	0.81
23	6% CSA 3% ZnO	30	3	546	5.55	3.1916	3.1862	0.0054	0.6092	5.4	6.3	0.7
24	6% CSA 3% ZnO	40	3	546	5.55	3.1862	3.1791	0.0071	0.5344	7.1	8.2	0.69
25	6% CSA 3% ZnO	20	4	728	4.16	3.2551	3.2305	0.0078	0.49	7.8	12	1.51
26	6% CSA 3% ZnO	30	4	728	4.16	3.2305	3.2265	0.004	0.7242	4	6.2	0.51

(continued)

Table 4 (continued)

Sl. No.	Composition of AA 5083	Load (N)	Sliding velocity (m/s)	Sliding speed (rpm)	Cumulative Time (sec)	Initial mass (m1)	Final mass (m2)	Wear Loss (Δm)	Coefficient of friction (Ff/N) (μ)	Wear rate Δm/L × 10^{-8} (m/L) (N/m)	Volumetric wear rate (wv × 10) [Δm/ρt] (mm^3/s)	Specific wear rate (ws × 10^{-1}) [wv/vs FN] (mm^3/N-m)
27	6% CSA 3% ZnO	40	4	728	4.16	3.2265	3.2259	0.0006	0.6656	0.6	0.9	0.06
28	9% CSA 3% ZnO	20	2	364	8.33	3.0084	3.0017	0.0067	0.79	6.7	5.6	1.39
29	9% CSA 3% ZnO	30	2	364	8.33	3.0009	2.9927	0.0082	0.5717	8.2	6.8	1.14
30	9% CSA 3% ZnO	40	2	364	8.33	3.9927	3.9835	0.0085	0.605	8.5	7.1	0.88
31	9% CSA 3% ZnO	20	3	546	5.55	3.012	3.0084	0.0036	0.7188	3.6	4.5	0.75
32	9% CSA 3% ZnO	30	3	546	5.55	3.9835	3.9787	0.0048	0.6392	4.8	6	0.67
33	9% CSA 3% ZnO	40	3	546	5.55	3.9783	3.9722	0.0061	0.5856	6.1	7.6	0.63
34	9% CSA 3% ZnO	20	4	728	4.16	3.0216	3.0146	0.007	0.6125	7.0	11.6	1.46
35	9% CSA 3% ZnO	30	4	728	4.16	3.0146	3.0126	0.002	0.7092	2.0	3.3	0.28
36	9% CSA 3% ZnO	40	4	728	4.16	3.0126	3.0122	0.0004	0.7769	0.4	0.7	0.04

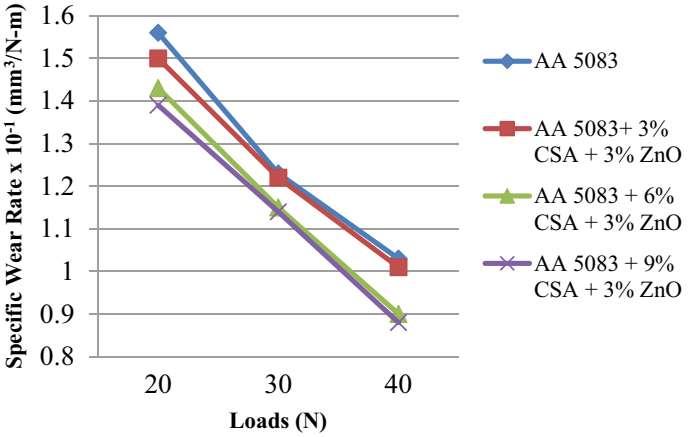

Fig. 3 Variation of aluminium alloy 5083 based composite specific wear rate with load

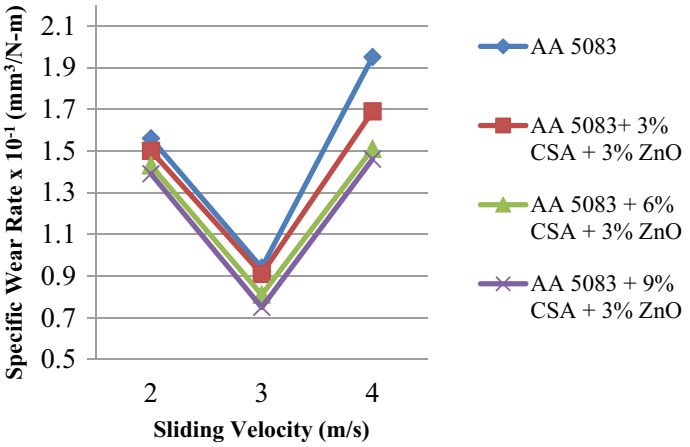

Fig. 4 Variation of aluminium alloy 5083 based composite specific wear rate with sliding velocity

4.3 Wear Mechanism

Multiple factors contribute to the specimens effective wear. Increased load causes hard asperities of the counter surface to penetrate the softer pin surface, micro cracking of the subsurface, and deformation and fracture of softer asperities. Beyond each composite critical load, the wear rate increases dramatically. The transition load is when a specific wear rate suddenly increases [23].

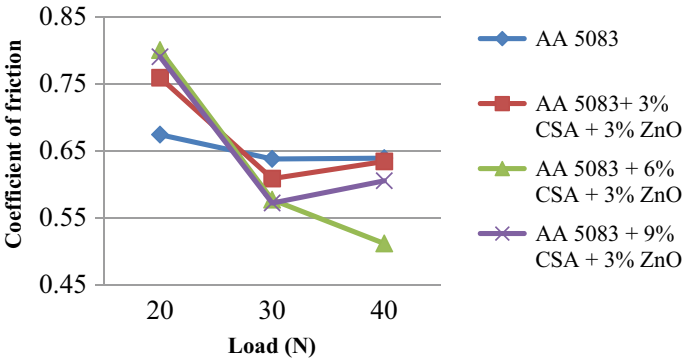

Fig. 5 Variation of aluminium alloy 5083 based composite coefficient of friction with Load

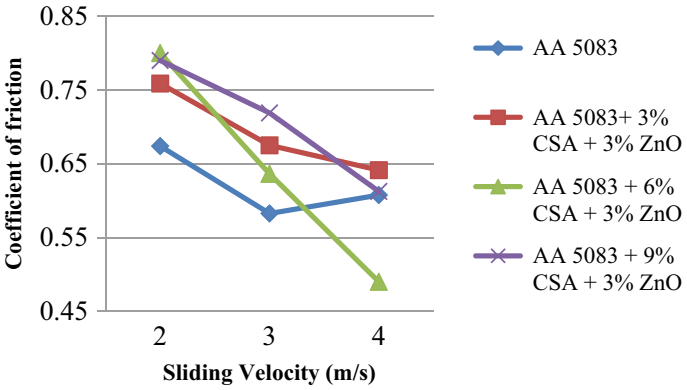

Fig. 6 Variation of aluminium alloy 5083 based composite coefficient of friction with sliding velocity

4.4 SEM Worn-Out Sample Images of AA 5083 Hybrid Composites

After Wear test worn-out samples were tested are shown in Fig. 7a AA 5083, Fig. 7b AA 5083 with 3% CSA + 3%ZnO, Fig. 7c AA 5083 with 6% CSA + 3%ZnO, Fig. 7d AA 5083 with 9% CSA + 3%ZnO.

AA 5083 HBMMCs are susceptible to delamination and adhesive wear as wear mechanisms. Here, it is described how surface morphology relates to each of the processes. Analyzed is a comparative research of hybrid composites made of 3%, 6%, and 9% CSA and 3% ZnO and 5083 aluminium. Unreinforced 5083 alloy and AA5083/CSA/ZnO hybrid composites are evaluated under constant load (40 N), sliding velocity (4 m/s), sliding time (4.16 min), and sliding distance conditions.

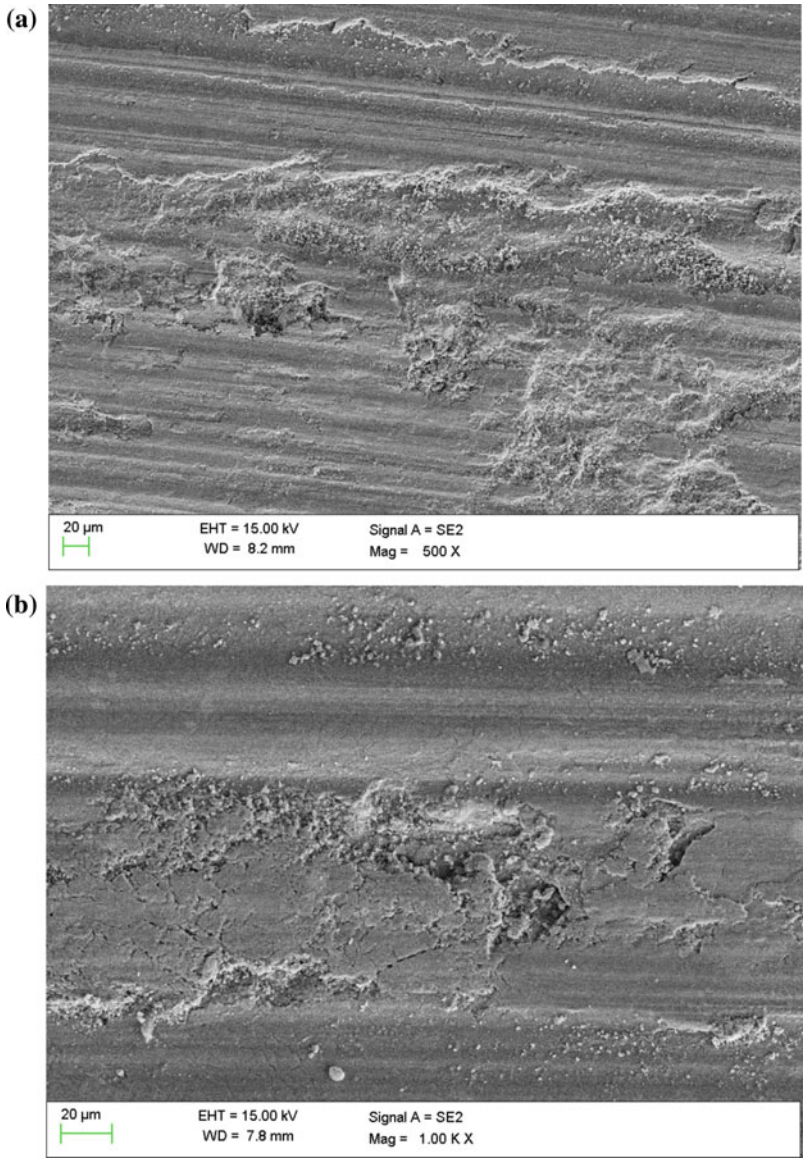

Fig. 7 SEM Images of AA 5083 and its hybrid composites

The results of these tests are photographed in scanning electron microscope (SEM) images (1000 m).

Figure 7a–d shows SEM micrographs and enlarged morphologies of AA 5083 matrix, CSA, and ZnO/AA 5083 hybrid composites at 40 N. AA5083/CSA/ZnO hybrid composites scratch less than AA5083. At 40 N, composites wear with large

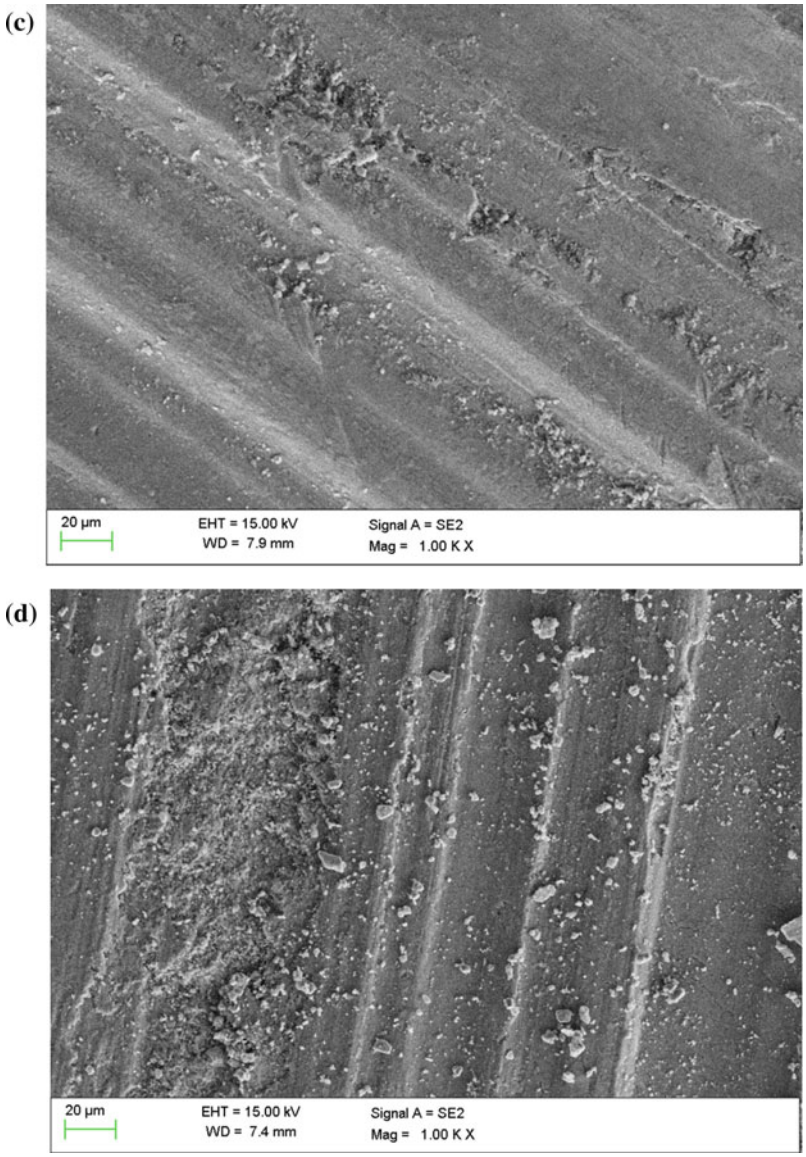

Fig. 7 (continued)

grooves and debris. The magnified morphology shows the AA5083/CSA/ZnO hybrid composites low applied load wear mechanism. Figure 7b–d reveal that micro-cutting and abrasive wear are the primary wear mechanisms Fig. 7d. The rather minor delamination layer occurrence of AA 5083/9% CSA/3% ZnO hybrid composite

demonstrated significantly increased wear resistance, which is comparable to Fig. 7d [24].

When the increased load is 40 N, layers of delamination attach to worn surfaces, as seen in Fig. 7a–d. At 40 N and 4 m/s sliding velocity, AA5083/CSA/ZnO hybrid composites show substantial to wear. Figure 7b–d show the enlarged morphology of the worn surfaces of AA5083/CSA/ZnO hybrid composites under 40 N loads.

CSA hard reinforcement changed pin and disc contact characteristics. The AA 5083 matrix was worn out first due to the hardness difference between the reinforcement and matrix. Grooves are formed as a result of debris being removed and pushed into ridges along the direction of sliding during the wear process. The deficiency of AA 5083 matrix increased the load-bearing function of CSA and ZnO particles and desquamation. Desquamated CSA/ZnO and AA 5083 matrix altered wear behaviours and generated abrasive wear. As sliding speed increased, AA5083/CSA/major ZnO wear mechanism changed from abrasion to adhesion. In the pin and disc counter body wear system, shear stress desquamated the AA5083 matrix, causing periodic plastic deformation of the AA5083/CSA/ZnO hybrid composite. Adhesion wear and a delamination layer were generated as a result of stress concentration between the pin and the disc. These features provided to shield the composite from further friction and to increase its wear resistance [25].

Figure 7 AA5083/CSA/ZnO hybrid composite is economical, efficient, and high wear resistant. Figure 7b–d Co-efficient of friction and Fig. 7b wear loss of AA 5083 matrix and AA5083/CSA/ZnO hybrid composite at various loads and sliding velocities. CSA and ZnO changed the pin-disc interaction properties. Due to the hardness discrepancy between the reinforcement, The adhesion wear delamination layer improved the composites wear resistance. Considering its economy, efficiency, and good wear resistance, the hot-press sintered AA5083/CSA/ZnO hybrid composite can be widely utilized in wear resistance applications.

4.5 Machine Learning (ML)

Open source ML and data visualisation system evaluated data. These metrics represent ANNs and provided outputs in terms of Specific Wear Rate (SWR). Per sample, the algorithm estimated Specific Wear Rate (SWR) using RF, NN, and kNN. Table 5 displays ML training parameters.

Random Forest (RF) is the most suitable assessment method, the estimate that was created by (just) the NN methodology was provided in that figure. This is because the Standard Deviation percentage ($\sigma\%$) of Table 6 indicates that the RF is the most appropriate evaluation method. The NN demonstrates a good connection between the experimental dataset and the predicted Specific Wear Rate with a value of 32% and 37% for AA 5083 hybrid composites. However, this correlation is not perfect (SWR).

Table 5 Parameters for machine learning methods

Random Forest	
Number of trees	15
Fixed seed for random generator	32
Do not split subset smaller than	5
Neural network	
Learning speed	0.6
Inertial coefficient	0.5
Test mass tolerance	0.02
Tolerance of the learning set	0.03
Number of layers	8
k-Nearest Neighbours (kNN)	
Metric	Chebyshev
Number of neighbor	2
Weight	Uniform

Table 6 displays the Mean value (μ), the Standard Deviation (σ), and the Relative Standard Deviation (σ %) to illustrate the variability of the overall value and compare the various techniques.

This prediction ensures a substantial coincidence in SWR averages (0.98 vs. 0.96) and variability.

Additionally, it seems that any Random Forest (RF) approach under examination may provide a reliable estimate. Figure 8 illustrates this feature by showing values from the various approaches (RF, NN, and kNN) in the context of, for instance, AA5083 hybrid composites.

Even though the specimens were taken from identical tribological conditions, this result may be seen as being more than suitable since the experimental results were subject to some inherent variability ($\sigma = 0.96$). Even while it is also clear that there is a trend toward a decrease overall, this variability was translated via the ML procedure. Neither as a structure nor during training, ML algorithms have not been optimized. Without going into specifics of AI Methods, this decision is tied to an investigative technique that aims to demonstrate their universal applicability.

The correlation between measurements and estimates as predicted by RF, NN, and KNN is shown point by point in Fig. 9. It demonstrates the ability of the Machine Learning technique to identify correlation ($r = 0.92$ on RF, $r = 0.84$ on NN, and $r = 0.90$ on kNN). This excellent match is shown by the clustering of data around the diagonal. They also demonstrate that there are values that significantly vary from this linearity. The distribution of points above and below the line suggests no systemic errors in the estimate.

Table 7 Showed Random Forest (RF) R-square value is more than 0.92 and 0.90 on KNN and 0.84 on NN algorithms in machine learning. Compared with the least values of error MSE, MAE and RMSE, RF model is less and a good prediction algorithm in Machine Learning.

Table 6 Parameters in machine learning

S. No.	SWR	RF	NN	KNN
1	1.46	1.41	1.53	1.56
2	1.20	1.27	1.23	1.23
3	0.99	1.02	1.02	1.03
4	1.02	1.22	0.93	0.94
5	0.99	1.05	0.81	0.90
6	0.95	0.61	0.69	0.73
7	1.48	1.61	1.82	1.95
8	1.04	0.92	0.99	1.43
9	1.05	0.81	0.85	1.55
10	1.35	1.57	1.53	1.50
11	1.16	1.34	1.23	1.22
12	0.98	1.03	1.02	1.01
13	0.97	1.14	0.93	0.91
14	0.75	1.02	0.81	0.73
15	0.72	0.63	0.69	0.64
16	1.19	1.40	1.82	1.69
17	0.44	0.95	0.99	0.55
18	0.47	0.47	0.85	0.15
19	1.37	1.45	1.46	1.43
20	1.16	1.18	1.19	1.15
21	0.94	0.95	0.96	0.90
22	0.96	1.02	0.86	0.81
23	0.73	0.92	0.71	0.70
24	0.71	0.63	0.67	0.69
25	1.40	1.38	1.60	1.51
26	0.43	0.70	0.53	0.51
27	0.66	0.43	0.10	0.06
28	1.33	1.14	1.41	1.39
29	1.16	0.83	1.15	1.14
30	0.98	0.67	0.89	0.88
31	0.81	0.71	0.78	0.75
32	0.68	0.75	0.69	0.67
33	0.70	0.53	0.66	0.63
34	1.31	1.05	1.48	1.46
35	0.43	0.53	0.40	0.28
36	0.44	0.04	0.05	0.04
Mean (μ)	0.96	0.96	0.98	0.96

(continued)

Table 6 (continued)

S. No.	SWR	RF	NN	KNN
St Dev (σ)	0.31	0.36	0.42	0.47
St Dev (σ%)	32	37	43	49

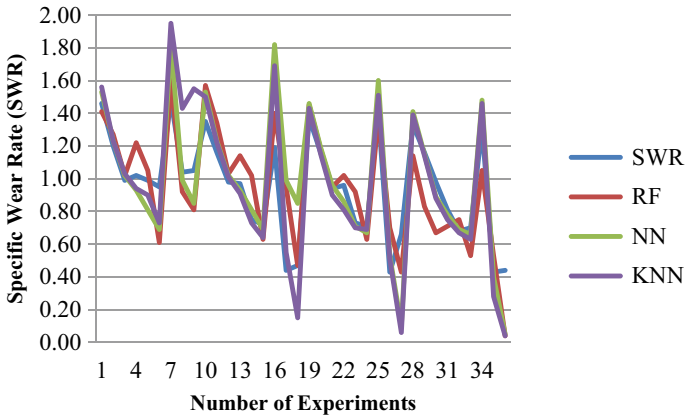

Fig. 8 Experimental SWR versus ML for AA 5083 and its hybrid composite

4.6 Artificial Neural Network (MLP Model)

The experimental data on AA 5083 composites was used to produce the data for training the ANN Multilayer Preceptron (MLP) model. A dataset consisting of a total of ($9 \times 4 = 36$) samples were collected, 3 for each combination of sample materials, specific wear rate and other parameters with six different inputs Load, Sliding velocity, Sliding speed, coefficient of friction, Cumulative time and % reinforcement as inputs and Specific Wear Rate as output (26 Samples) was used to train the ANN-MLP model. 15% (5 Samples) of total input data was used for test data and cross-validation (5 Samples). Cross-validation stops network training. This approach detects data error and stops training when it increases. The best generalization occurs here. Figure 12 specifies cross-validation and testing data sets. Figure 10 shows the MLP structure design, output, input, transfer functions, and hidden layers.

A wide range of composites were tested for Specific Wear Rate. Data has been statistically and ML-analyzed. ANN-MLP method improved specific wear rate prediction.

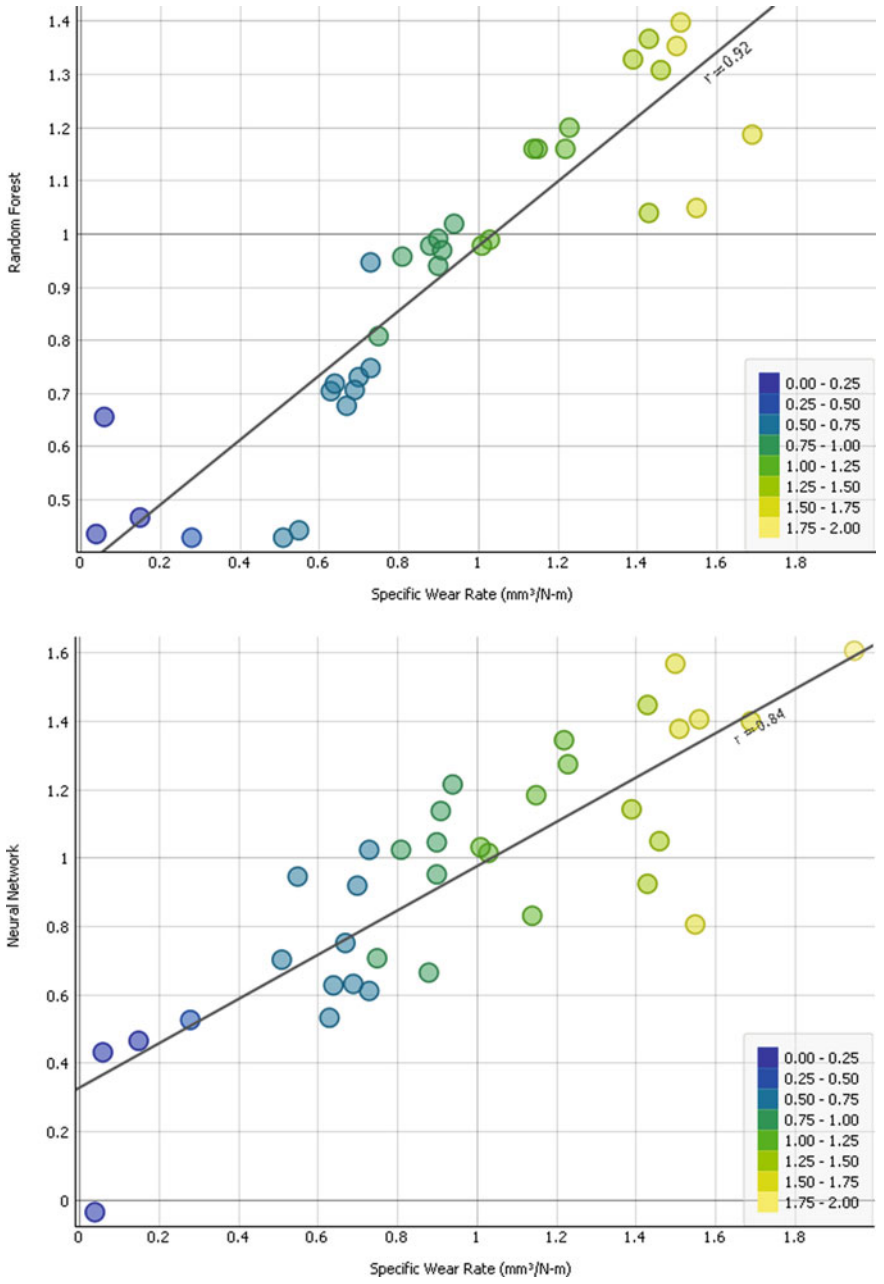

Fig. 9 The correlation between specific wear rate data and estimates is predicted by RF, NN, and kNN techniques

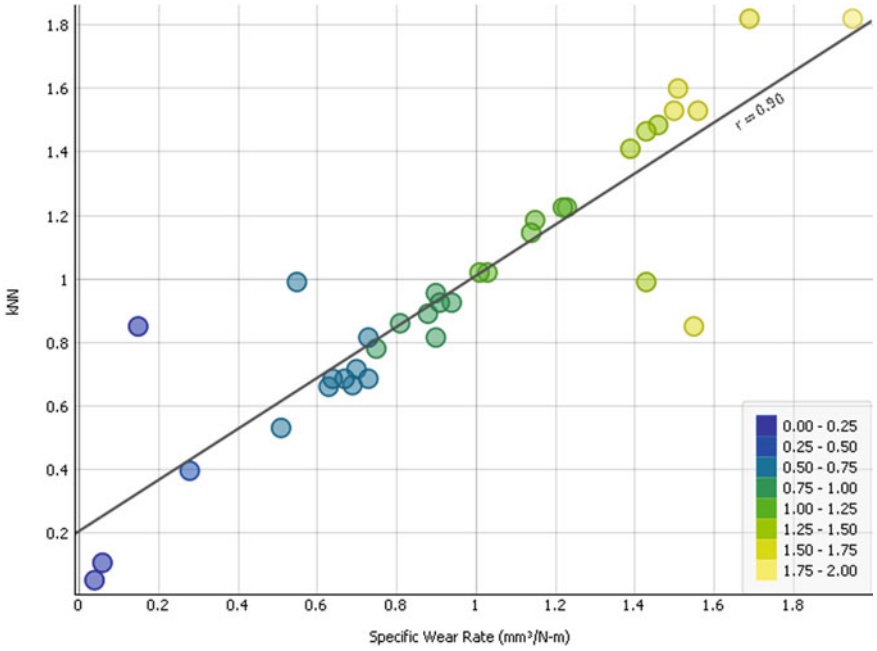

Fig. 9 (continued)

Table 7 Comparison of test results ML

Model	MSE	RMSE	MAE	R^2
Random Forest	0.040	0.201	0.099	0.92
Neural network	0.064	0.254	0.198	0.84
kNN	0.048	0.219	0.149	0.90

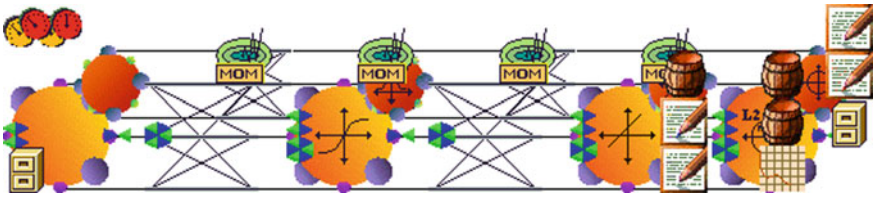

Fig. 10 Multilayer preceptron (MLP) network architecture design

4.7 ANN-MLP Training and Testing

The training results indicate good functionality and a low inaccuracy of 0.00000496 at 2991 epochs. 2991 epochs later, training is complete. Mean Square Error MSE curve

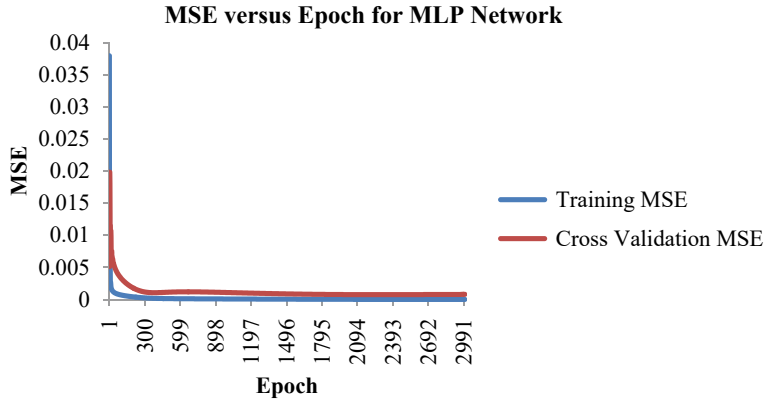

Fig. 11 Training performance of the multilayer preceptron (MLP) network

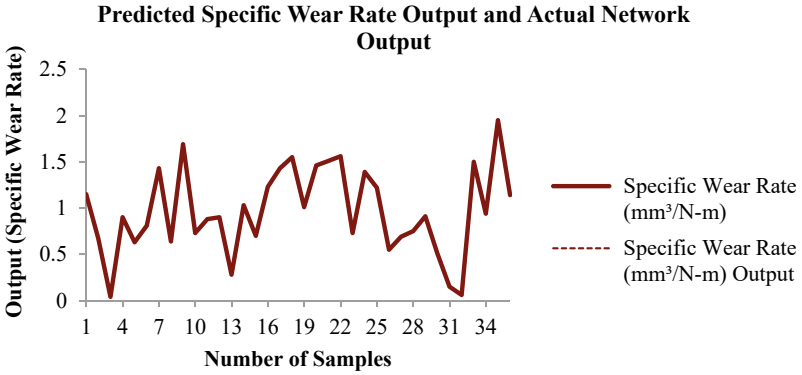

Fig. 12 Testing Performance of the multilayer preceptron (MLP) network

shows weight decay, indicating superior functioning. The network's functioning is further analyzed. Figure 11 shows training and cross-validation results.

The testing operation's MSE is 0.00001599 and MAE is 0.00276. This indicates good performance. NMSE is 0.0000749, while r is 0.99996. The reason that the components are so close to forming a straight line, as shown by the linear correlation value of 0.99996, suggests that there is a strong link between them. Figure 12 demonstrates the projected MLP Specific Wear Rate network output matches the actual rate.

5 Conclusion

The following are the findings of the present investigation:

Coconut Shell Ash (CSA) can be utilised to manufacture Aluminium Metal Matrix Hybrid Composite. It can replace aluminum-heavy materials. CSA can be used to make composites from agricultural waste. This helps with CSA storage and disposal.

Stir Casting successfully incorporates CSA and ZnO into aluminium alloy 5083. This approach produced hybrid composites with 3, 6, and 9 wt% CSA and 3 wt% ZnO. Stir Casting successfully incorporates CSA and ZnO into aluminium alloy 5083.

Specific wear rate reduces with increasing CSA weight%, and ZnO particles have outstanding tribological features, the least wear loss and coefficient of friction in all test settings. Increasing CSA and ZnO particles lowers Aluminium 5083 alloy friction. 6% CSA and 3% ZnO hybrid composites increase friction coefficient at 20 N and 30 N, 2 m/s sliding speed. Poor interfacial bonding between the reinforcement and matrix alloy increases friction.

At applied load 40 N, micro-cutting and abrasive wear were the major AA5083/CSA/ZnO wear mechanisms. Load 40 N supported micro-cutting and adhesion wear. Adhesion wear created a delamination layer that increased composite wear resistance.

Mchine learning methods predicted AA5083 hybrid composites wear rate. Using machine learning methods, the suggested model predicted wear.

Machine learning uses RF, NN, and KNN to predict SWR. NN had the lowest success rate, but RF and KNN were equal; R-squared was 0.92 in RF, 0.84 in NN, and 0.90 in KNN. The RF method had improved RMSE and MAE values. The RF method developed the most efficient model among the presented machine learning techniques for predicting wear rate.

To increase the prediction accuracy and R-square value ANN (MLP) Multilayer Perceptron neural network was used to train and test the network.

Accuracy and error percentage compared in both results for the regression coefficient of machine learning and artificial neural network with two models ML-NN design and ANN-MLP design Specific Wear Rate was adopted.

The regression R-square values for this network were 0.84–0.99. An Error of 0.16 to 0.01 and prediction accuracy of 84% to 99% and 15% improved by using this Multilayer Perceptron (MLP) network is more accurate for AA 5083 hybrid composites and any other types of materials. So, therefore the Artificial Neural Network can be used for predicting tribological parameters and showed good coincidence with the experimental results of these AA 5083 hybrid composites.

This results in the conclusion that both ML and ANN may be useful in preparing an AA 5083 hybrid composite with the optimal ratio of reinforcing elements.

References

1. Ikumapayi OM, Akinlabi ET, Pal SK, Majumdar JD (2019) A survey on reinforcements used in friction stir processing of aluminium metal matrix and hybrid composites. Proc Manuf 35:935–940

2. Sudherson DPS, Sunil J (2020) Dry sliding wear behaviour of novel AA5083-cadmium alloy prepared by stir casting process. Mater Today: Proc 21:142–147
3. Zhang T, Li DY (2001) Improvement in the resistance of aluminum with yttria particles to sliding wear in air and in a corrosive medium. Wear 251(1–12):1250–1256
4. Arulraj M, Palani PK (2018) Parametric optimization for improving impact strength of squeeze cast of hybrid metal matrix (LM24–SiC p–coconut shell ash) composite. J Braz Soc Mech Sci Eng 40(1):2
5. Ma X, Chang PR, Yang J, Yu J (2009) Preparation and properties of glycerol plasticized-pea starch/zinc oxide-starch bionanocomposites. Carbohyd Polym 75(3):472–478. https://doi.org/10.1016/j.carbpol.2008.08.007
6. Tun KS, Jayaramanavar P, Nguyen QB, Chan J, Kwok R, Gupta M (2012) Investigation into tensile and compressive responses of Mg–ZnO composites. Mater Sci Technol 28(5):582–588
7. Selvam B, Marimuthu P, Narayanasamy R, Anandakrishnan V, Tun KS, Gupta M, Kamaraj M (2014) Dry sliding wear behaviour of zinc oxide reinforced magnesium matrix nano-composites. Mater Des 58:475–481. https://doi.org/10.1016/j.matdes.2014.02.006
8. Jasim AH, Joudi WM, Radhi NS, Saud AN (2020) Mechanical properties and wear characteristic of (aluminum-zinc oxide) metal matrix composite prepared using stir casting process. Mater Sci Forum 1002:175–184. Trans Tech Publications Ltd
9. Raju RSS, Panigrahi MK, Ganguly RI, Rao GS (2017) Investigation of tribological behavior of a novel hybrid composite prepared with Al-coconut shell ash mixed with graphite. Metall Mater Trans A 48(8):3892–3903. https://doi.org/10.1007/s11661-017-4139-1
10. Tang F, Wu X, Ge S, Ye J, Zhu H, Hagiwara M, Schoenung JM (2008) Dry sliding friction and wear properties of B4C particulate-reinforced Al-5083 matrix composites. Wear 264(7–8):555–561. https://doi.org/10.1016/j.wear.2007.04.006
11. Thiyaneshwaran N, Sureshkumar P (2013) Microstructure, mechanical and wear properties of aluminum 5083 alloy processed by equal channel angular extrusion. Int J Eng Res Technol 2:17–24
12. Bathula S, Saravanan M, Dhar A (2012) Nanoindentation and wear characteristics of Al 5083/SiCp nanocomposites synthesized by high energy ball milling and spark plasma sintering. J Mater Sci Technol 28(11):969–975
13. Madakson PB, Yawas DS, Apasi A (2012) Characterization of coconut shell ash for potential utilization in metal matrix composites for automotive applications. Int J Eng Sci Technol 4(3):1190–1198
14. Daramola OO, Adediran AA, Fadumiye AT (2015) Evaluation of the mechanical properties and corrosion behaviour of coconut shell ash reinforced aluminium (6063) alloy composites. Leonardo Electron J Pract Technol 27:107–119
15. Agunsoyea JO, Talabib SI, Belloa SA, Awec IO (2014) The effects of Cocos Nucifera (coconut shell) on the mechanical and tribological properties of recycled waste aluminium can composites. Tribol Industry 36(2)
16. Xue D, Balachandran PV, Hogden J, Theiler J, Xue D, Lookman T (2016) Accelerated search for materials with targeted properties by adaptive design. Nat Commun 7(1):1–9. https://doi.org/10.1038/ncomms11241
17. Xiong J, Shi SQ, Zhang TY (2020) A machine-learning approach to predicting and understanding the properties of amorphous metallic alloys. Mater Des 187:108378. https://doi.org/10.1016/j.matdes.2019.108378
18. Sarica A, Cerasa A, Quattrone A (2017) Random Forest algorithm for the classification of neuroimaging data in Alzheimer's disease: a systematic review. Front Aging Neurosci 9:329. https://doi.org/10.3389/fnagi.2017.00329
19. Abd Jalil K, Kamarudin MH, Masrek MN (2010) Comparison of machine learning algorithms performance in detecting network intrusion. In: 2010 international conference on networking and information technology. IEEE, pp 221–226
20. Tretyakov K (2004) Machine learning techniques in spam filtering. In: Data mining problem-oriented seminar, MTAT, vol 3, No 177, pp 60–79. Citeseer

21. Shataee S, Kalbi S, Fallah A, Pelz D (2012) Forest attribute imputation using machine-learning methods and ASTER data: comparison of k-NN, SVR and random forest regression algorithms. Int J Remote Sens 33(19):6254–6280. https://doi.org/10.1080/01431161.2012.682661
22. Nagaraj A, Gopalakrishnan S (2021) A study on mechanical and tribological properties of aluminium 1100 alloys 6% of RHAp, BAp, CSAp, ZnOp and egg shellp composites by ANN. SILICON 13(10):3367–3376
23. Mazahery A, Shabani MO (2012) Study on microstructure and abrasive wear behavior of sintered Al matrix composites. Ceram Int 38(5):4263–4269
24. Alizadeh A, Abdollahi A, Biukani H (2015) Creep behavior and wear resistance of Al 5083 based hybrid composites reinforced with carbon nanotubes (CNTs) and boron carbide (B4C). J Alloy Compd 650:783–793
25. Zhao Q, Liang Y, Zhang Z, Li X, Ren L (2016) Microstructure and dry-Sliding wear behavior of B4C ceramic particulate reinforced Al 5083 matrix composite. Metals 6(9):227